nature medicine

ARTICLES

https://doi.org/10.1038/s41591-018-0059-x

The human heart contains distinct macrophage subsets with divergent origins and functions

Geetika Bajpai[1], Caralin Schneider[1], Nicole Wong[1], Andrea Bredemeyer[1], Maarten Hulsmans[2], Matthias Nahrendorf[2], Slava Epelman[3], Daniel Kreisel[4], Yongjian Liu[5], Akinobu Itoh[4], Thirupura S. Shankar[6], Craig H. Selzman[7], Stavros G. Drakos[8] and Kory J. Lavine[1,9,10]*

Paradigm-shifting studies in the mouse have identified tissue macrophage heterogeneity as a critical determinant of immune responses. In contrast, surprisingly little is known regarding macrophage heterogeneity in humans. Macrophages within the mouse heart are partitioned into CCR2− and CCR2+ subsets with divergent origins, repopulation mechanisms, and functions. Here, we demonstrate that the human myocardium also contains distinct subsets of CCR2− and CCR2+ macrophages. Analysis of sex-mismatched heart transplant recipients revealed that CCR2− macrophages are a tissue-resident population exclusively replenished through local proliferation, whereas CCR2+ macrophages are maintained through monocyte recruitment and proliferation. Moreover, CCR2− and CCR2+ macrophages have distinct functional properties, analogous to reparative CCR2− and inflammatory CCR2+ macrophages in the mouse heart. Clinically, CCR2+ macrophage abundance is associated with left ventricular remodeling and systolic function in heart failure patients. Collectively, these observations provide initial evidence for the functional importance of macrophage heterogeneity in the human heart.

Over the past 40 years the prevailing view has been that tissue macrophages originate from circulating blood monocytes. Recently, a growing body of literature has challenged this dogma and revolutionized our understanding of macrophage heterogeneity and origins. Studies performed in mouse models have provided evidence that tissue macrophages represent a diverse population of cells originating from a variety of lineages[1–3]. In the mouse, many tissue-resident macrophages in the brain, skin, liver, kidney, lung, and heart first enter their respective tissues during embryonic development and persist into adulthood independent of monocyte recruitment[4–12]. Embryonic-derived macrophages are long-lived and replenished locally independent of peripheral monocyte input through cell proliferation[4,13]. In contrast, classically described macrophages originate from definitive hematopoietic progenitors located within the bone marrow and spleen and are replenished under homeostatic and inflammatory conditions through monocyte recruitment in a CCR2 (receptor for CCL2/MCP1 and CCL7/MCP3)-dependent manner[6,7]. These advancements in knowledge relied on the establishment of genetic lineage tracing, parabiosis, and cell tracking strategies only available in rodent systems[14–16].

While tissue-resident macrophage populations and their exact embryonic origins continue to be defined across a variety of organs and tissues, it is immediately apparent that macrophage origin is a critical determinant of cell behavior. This is particularly important as macrophages of distinct origin often coexist within tissues[11]. For example, the heart contains several different macrophage subsets that can be differentiated through genetic lineage tracing and cell surface expression of CCR2. By employing flow cytometry, lineage tracing, and parabiosis strategies, we previously demonstrated that the mouse heart contains distinct CCR2− and CCR2+ macrophage populations. CCR2− macrophages are derived from primitive yolk sac and fetal monocyte progenitors. CCR2− macrophages enter the heart during embryonic development and, in the absence of disease, are maintained throughout life independent of monocyte recruitment. In contrast, CCR2+ macrophages originate from definitive hematopoietic progenitors, are recruited to the heart after the first few weeks of life, and are maintained through monocyte recruitment and subsequent proliferation[8,17,18].

Importantly, CCR2− and CCR2+ macrophages have distinct functions in the heart. CCR2− macrophages are involved in various forms of tissue remodeling such as coronary development, postnatal coronary growth, and cardiac regeneration[17,18]. For example, following neonatal cardiomyocyte injury, CCR2− macrophages orchestrate cardiac tissue regeneration and functional recovery of the heart through expansion of the coronary vasculature, cardiomyocyte proliferation, and physiological cardiomyocyte hypertrophy. In the absence of CCR2− macrophages, the pediatric mouse heart demonstrates little regenerative capacity. Within the resting adult heart, the exact functions of CCR2+ macrophages are not completely defined. However, it is likely that CCR2+ macrophages participate in the initiation of inflammation. CCR2+ macrophages are activated following ischemia reperfusion injury in a TLR9-dependent

[1]Center for Cardiovascular Research, Division of Cardiology, Department of Medicine, Washington University School of Medicine, Saint Louis, MO, USA. [2]Center for Systems Biology, Massachusetts General Hospital, Harvard Medical School, Boston, MA, USA. [3]Peter Munk Cardiac Center, Ted Rogers Center for Heart Failure Research, Toronto General Hospital, University of Toronto, Toronto, Ontario, Canada. [4]Department of Surgery, Washington University School of Medicine, Saint Louis, MO, USA. [5]Department of Radiology, Washington University School of Medicine, Saint Louis, MO, USA. [6]Nora Eccles Harrison Cardiovascular Research and Training Institute (CVRTI), University of Utah School of Medicine, Salt Lake City, UT, USA. [7]Division of Cardiothoracic Surgery & Nora Eccles Harrison Cardiovascular Research and Training Institute (CVRTI), University of Utah School of Medicine, Salt Lake City, UT, USA. [8]Division of Cardiovascular Medicine & Nora Eccles Harrison Cardiovascular Research and Training Institute (CVRTI), University of Utah School of Medicine, Salt Lake City, UT, USA. [9]Department of Developmental Biology, Washington University School of Medicine, Saint Louis, MO, USA. [10]Department of Immunology and Pathology, Washington University School of Medicine, Saint Louis, MO, USA. *e-mail: klavine@wustl.edu

manner and mediate neutrophil extravasation into the injured myocardium through production of neutrophil chemokines including CXCL2 and CXCL5[19].

Collectively, these studies have established that in mice the heart contains a heterogeneous population of functionally distinct macrophages with remarkable effects on cardiovascular disease pathogenesis. However, macrophage heterogeneity in human tissues remains largely unexplored. In this study, we tested the hypothesis that the human heart contains distinct macrophage populations that are functionally analogous to mouse cardiac CCR2− and CCR2+ macrophages.

Results

The human heart contains distinct subsets of CCR2− and CCR2+ macrophages. To define appropriate cell surface markers for human cardiac macrophages, we performed immunostaining on left ventricular myocardial specimens obtained from subjects with dilated and ischemic cardiomyopathies. Transmural left ventricular specimens were collected at the time of left ventricular assist device (LVAD) implantation or heart transplantation. All specimens were obtained from either the apical or lateral left ventricular walls. We first tested whether cardiac macrophages express CD14, a GPI anchored TLR4 coreceptor preferentially expressed on human monocytes and macrophages[20]. Dual immunostaining for CD68 (pan-macrophage marker) and CD14 revealed that human cardiac macrophages uniformly express CD14 (Fig. 1a). Quantification of CD14+CD68+ cells in specimens obtained from subjects with dilated cardiomyopathy (DCM) and ischemic cardiomyopathy (ICM) revealed that the vast majority of cardiac macrophages are CD14+ (94.1 and 94.4%, respectively) (Fig. 1b). Based on the finding that human cardiac macrophages uniformly express CD14, we devised a flow cytometry gating scheme to identify and characterize human cardiac macrophage populations.

Previously, we and others have performed detailed lineage tracing, flow cytometry, and transcriptomic analyses to define cell surface markers for cardiac macrophages in the mouse including CD45, CD64, MHC-II and CCR2[8,17,18,21,22]. To test the hypothesis that human cardiac macrophages can be identified using an evolutionarily conserved set of cell surface markers, we performed the following experiments. Flow cytometry analysis revealed that CD14+ cells present in the human heart coexpress both CD45 (common leukocyte antigen) and CD64 (Fc gamma receptor 1A) (Fig. 1c). CD64 is an evolutionarily conserved receptor that is exclusively expressed on mouse and human monocytes and macrophages. CD64 is not expressed on other myeloid cells including neutrophils, eosinophils, or dendritic cells[20,23]. Using a gating strategy similar to that employed in our previous studies focused on mouse cardiac macrophages[8], we demonstrated that CD14+CD45+CD64+ cells can be divided into three distinct subsets based on the expression of HLA-DR (human homologue of MHC-II) and CCR2: CCR2+HLA-DR^{low}, CCR2+HLA-DR^{high}, and CCR2−HLA-DR^{high} cells. The distribution of these cell types did not differ between ICM and DCM (Supplementary Fig. 1a). To more precisely define the identity of these cell populations, we performed further flow cytometry assays examining the expression of established cell markers. Previous studies have demonstrated that MertK (MER proto-oncogene tyrosine kinase) is an evolutionarily conserved marker specific for mouse and human macrophages[20,23]. Compared to isotype control, MertK staining could only be detected on CCR2+HLA-DR^{high} and CCR2−HLA-DR^{high} cells, suggesting that CCR2+HLA-DR^{high} and CCR2−HLA-DR^{high} cells represent macrophages and CCR2+HLA-DR^{low} cells are monocytes. Consistent with monocyte and macrophage identity, CCR2+HLA-DR^{low}, CCR2+HLA-DR^{high}, and CCR2−HLA-DR^{high} cells expressed both CD33 (Siglec-3, myeloid marker) and CD163 (monocyte/macrophage marker) and lacked expression of CD3 (T cell marker), CD19 (B cell marker), and CD56 (natural killer cell marker) (Fig. 1d).

To provide confirmatory evidence that human cardiac macrophages can be divided into CCR2− and CCR2+ subsets using a separate technique, we developed an immunostaining assay to identify CCR2− and CCR2+ macrophages in formalin-fixed, paraffin-embedded human heart tissue. For immunostaining experiments we identified monocytes and macrophages using CD68, a marker routinely used in clinical practice. Intracellular flow cytometry confirmed that CD45+CD14+CD64+ cells also expressed CD68 and that monocytes, CCR2− macrophages, and CCR2+ macrophages were found within the CD45+CD14+CD64+CD68+ gate (Supplementary Fig. 1b). Immunostaining with antibodies specific for CD64, CD68, and CCR2 revealed the presence of CD64+CD68+ CCR2− and CD64+CD68+CCR2+ cells within the left ventricular myocardium (Fig. 1e, Supplementary Fig. 1c). Together, these data demonstrate that the human heart contains a heterogeneous population of monocytes and macrophages that can be divided into distinct subsets based on the expression of CCR2 and HLA-DR.

Tissue localization of CCR2− and CCR2+ macrophages. To determine whether CCR2− macrophages and CCR2+ monocytes/macrophages occupy distant locations within the left ventricular myocardium, we performed CD68 and CCR2 immunostaining on specimens obtained from DCM and ICM subjects. Tissues were perfused with saline before fixation to remove intravascular immune cells including monocytes. Flow cytometry and immunostaining analyses indicated that tissue perfusion substantially reduced monocyte numbers and that the majority of CD68+ cells were CCR2−HLA-DR^{pos} and CCR2+HLA-DR^{pos} macrophages (Supplementary Fig. 2a–c). Rare monocytes (CCR2+HLA-DR^{neg}) were only found adjacent to blood vessels located within areas of dense fibrosis (Supplementary Fig. 2d). Within viable appearing areas of myocardium (defined by the absence of scar tissue) the majority of CD68+ cells represented CCR2− macrophages. Costaining with either CD34 or eNOS antibodies (vascular markers) revealed that CCR2− macrophages were closely associated with coronary endothelial cells (Supplementary Fig. 3a,d). In contrast, CCR2+ macrophages preferentially occupied areas containing scar or fibrotic tissue where they were found embedded in areas infiltrated with type I collagen (Supplementary Fig. 3b,d). We have previously demonstrated that mouse CCR2− and CCR2+ macrophages are activated in response to cardiomyocyte cell death[17,19]. To determine whether human CCR2− and CCR2+ macrophages might similarly recognize dying cardiomyocytes, we performed CD68, CCR2, and TdT-mediated dUTP nick end labeling (TUNEL) staining. CCR2− and CCR2+ macrophages were both present adjacent to TUNEL+ cardiomyocytes at equivalent ratios. However, areas of cell death were rare and the majority of CCR2− and CCR2+ macrophages were not located adjacent to TUNEL+ cardiomyocytes (Supplementary Fig. 3c,d).

CCR2− and CCR2+ macrophages are maintained through distinct mechanisms. To delineate whether human cardiac CCR2− and CCR2+ macrophages are maintained through similar or distinct mechanisms we measured contributions from peripheral monocyte recruitment and cell proliferation. We chose to focus on peripheral recruitment and cell proliferation as previous studies in the mouse have demonstrated that these activities represent the primary mechanisms responsible for maintenance and repopulation of mouse tissue macrophages[11].

To measure the contribution of peripheral monocyte recruitment to the maintenance of human cardiac CCR2− and CCR2+ macrophage subsets, we examined endomyocardial biopsy specimens obtained from sex-mismatched heart transplant recipients. All included endomyocardial biopsy specimens were obtained from male patients who received a heart from a female donor. The mean time from transplant was 8.8 years and none of the included biopsy

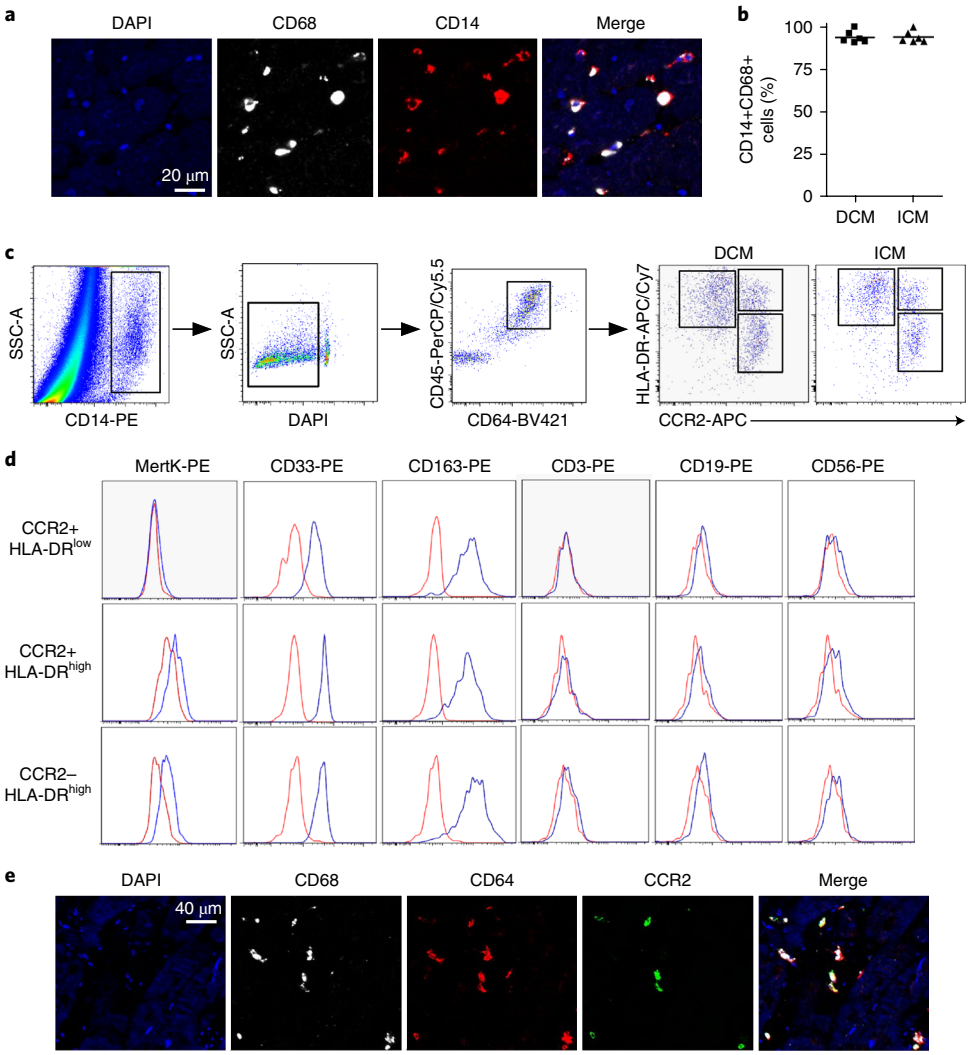

Fig. 1 | The human heart contains distinct populations of CCR2− and CCR2+ macrophages. a, Immunostaining of human cardiac macrophages (CD68, white) for CD14 (red). Blue, DAPI. **b**, Percentage of CD14+CD68+ cells in specimens obtained from subjects with DCM and ICM. Each data point ($n=6$) represents a biologically independent heart failure sample. The line indicates the mean value. **c**, Flow cytometry gating scheme utilized to identify and characterize cardiac macrophage populations. **d**, Flow cytometry plots showing expression of MertK (macrophage marker), CD33 and CD163 (monocyte/macrophage markers), CD3 (T cell marker), CD19 (B cell marker), and CD56 (natural killer cell marker) in CCR2+HLA-DR^{low}, CCR2−HLA-DR^{high}, and CCR2+HLA-DR^{high} cells. Red, isotype control; blue, indicated antibody. **e**, Immunostaining for CD68 (white), CD64 (red), and CCR2 (green) indicates that both CCR2− and CCR2+ macrophages are present within the left ventricular myocardium. These experiments were independently repeated three times with similar results. Blue, DAPI. **a**, Original magnification, ×400. **e**, Original magnification, ×200.

specimens showed evidence of rejection or allograft dysfunction (Supplementary Table 1). Using a combination of immunostaining for CD68 and CCR2 and in situ hybridization for Y chromosomes, we quantified the percentage of CCR2− and CCR2+ macrophages that were derived from the recipient avoiding intravascular CD68+ cells (Fig. 2a,b). Recipient-derived (Y chromosome+) macrophages were interpreted as originating from recruited monocytes. Consistent with being a tissue-resident population, only a small percentage of CCR2− macrophages (0.70 ± 1.4%) contained a Y chromosome. In contrast, 30.6 ± 16.8% of CCR2+ macrophages contained a Y chromosome, suggesting that peripheral monocyte recruitment represents an important mechanism by which CCR2+ macrophages are maintained in the human heart (Fig. 2c).

To examine whether cell proliferation also contributes to human cardiac CCR2− and CCR2+ macrophage maintenance, we performed immunostaining for CD68, CCR2, and Ki67 (Fig. 2d,e). Both CCR2− and CCR2+ macrophage populations displayed significant numbers of cells that were Ki67+, indicating that cell proliferation is an important mechanism of cell maintenance for each macrophage subset. However, CCR2+ macrophages displayed higher frequencies of Ki67+ cells compared to CCR2− macrophages (DCM: 29.0 ± 11.4% versus 17.2 ± 7.2%, $P<0.01$ and ICM: 30.3 ± 8.0% versus 11.1 ± 6.9%, $P<0.01$) (Fig. 2f). Together, these data suggest that CCR2− macrophages represent a tissue-resident population that is maintained through cell proliferation, while CCR2+ macrophages are maintained through a combination of monocyte recruitment and cell proliferation. These data are consistent with previous work suggesting that monocyte recruitment and local proliferation are important mechanisms contributing to macrophage expansion in the chronically failing mouse heart[22] and suggest that human cardiac CCR2+ macrophages may have higher turnover rates compared to human cardiac CCR2− macrophages.

Gene expression profiling of CCR2− macrophages, CCR2+ macrophages, and CCR2+ monocytes suggests differential cell origins and functions. To provide further evidence that human cardiac

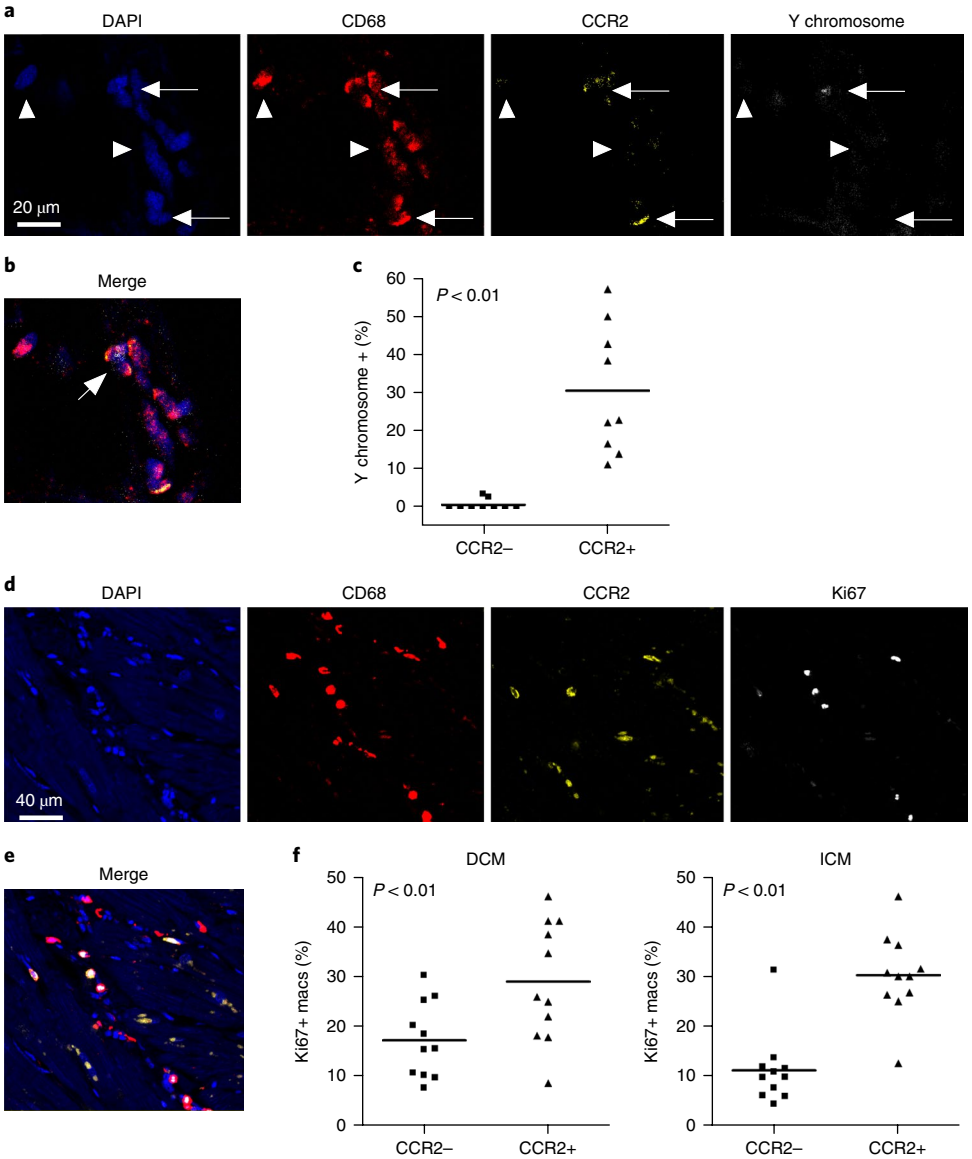

Fig. 2 | CCR2− and CCR2+ cardiac macrophage populations are maintained through distinct mechanisms. a, In situ hybridization and immunostaining of endomyocardial biopsy specimens obtained from recipients of sex-mismatched heart transplants ($n=9$). All specimens were obtained from male subjects who had received a heart from a female donor >1 year before biopsy. DAPI (blue), CD68 (red), CCR2 (yellow), and Y chromosome (white). Arrows, CCR2+ macrophages; arrowheads, CCR2− macrophages. **b**, Merged image from **a**. Original magnification, ×400. Arrow denotes CCR2+ macrophage containing a Y chromosome. **c**, Percentages of CCR2− and CCR2+ macrophages that contain a Y chromosome ($n=9$). Each data point represents a biologically independent biopsy specimen and the line refers to the mean value. Mann–Whitney test (two-sided), $P<0.0001$. **d**, Cell proliferation of CCR2− and CCR2+ macrophages, as assessed by immunostaining for CD68 (red), CCR2 (yellow), and Ki67 (white). Each data point represents a biologically independent heart failure specimen and the line refers to the mean value. Mann–Whitney test (two-sided): DCM, $P=0.0036$ and ICM, $P=0.006$. **e**, Merged image from **d**. Original magnification, ×200. **f**, Percentage of CCR2− and CCR2+ macrophages (macs) staining for Ki67 in hearts from DCM ($n=11$) and ICM ($n=11$) patients.

CCR2− and CCR2+ macrophages comprise functionally distinct macrophage populations, we performed transcriptomic profiling of RNA isolated from purified CCR2− macrophages ($n=19$ subjects), CCR2+ macrophages ($n=19$ subjects), and CCR2+ monocytes ($n=10$ subjects) using microarray technology. Macrophages and monocyte populations were isolated from subjects with DCM ($n=8$) and ICM ($n=11$) using flow cytometry-based cell sorting. Before performing our transcriptomic profiling studies, we examined the morphology of flow cytometry-sorted CCR2+HLA-DR^{low} monocytes, CCR2+HLA-DR^{high} macrophages, and CCR2−HLA-DR^{high} macrophages using cytospin preparations. Compared to CCR2+HLA-DR^{low} monocytes, CCR2+HLA-DR^{high} and CCR2−HLA-DR^{high} macrophage subsets displayed increased granularity consistent with known distinctions between monocyte and macrophage morphology. In addition, the morphology of CCR2+HLA-DR^{high} and CCR2−HLA-DR^{high} macrophages differed, with CCR2+HLA-DR^{high} macrophages being larger in size compared to CCR2−HLA-DR^{high} macrophages (Fig. 3a).

Consistent with the concept that CCR2− macrophages, CCR2+ macrophages, and CCR2+ monocytes represent distinct cell types, hierarchical clustering demonstrated that each cell population clustered tightly together. Furthermore, CCR2+ macrophages preferentially clustered with CCR2+ monocytes, suggesting that these populations are closely related (Fig. 3b). These data are consistent

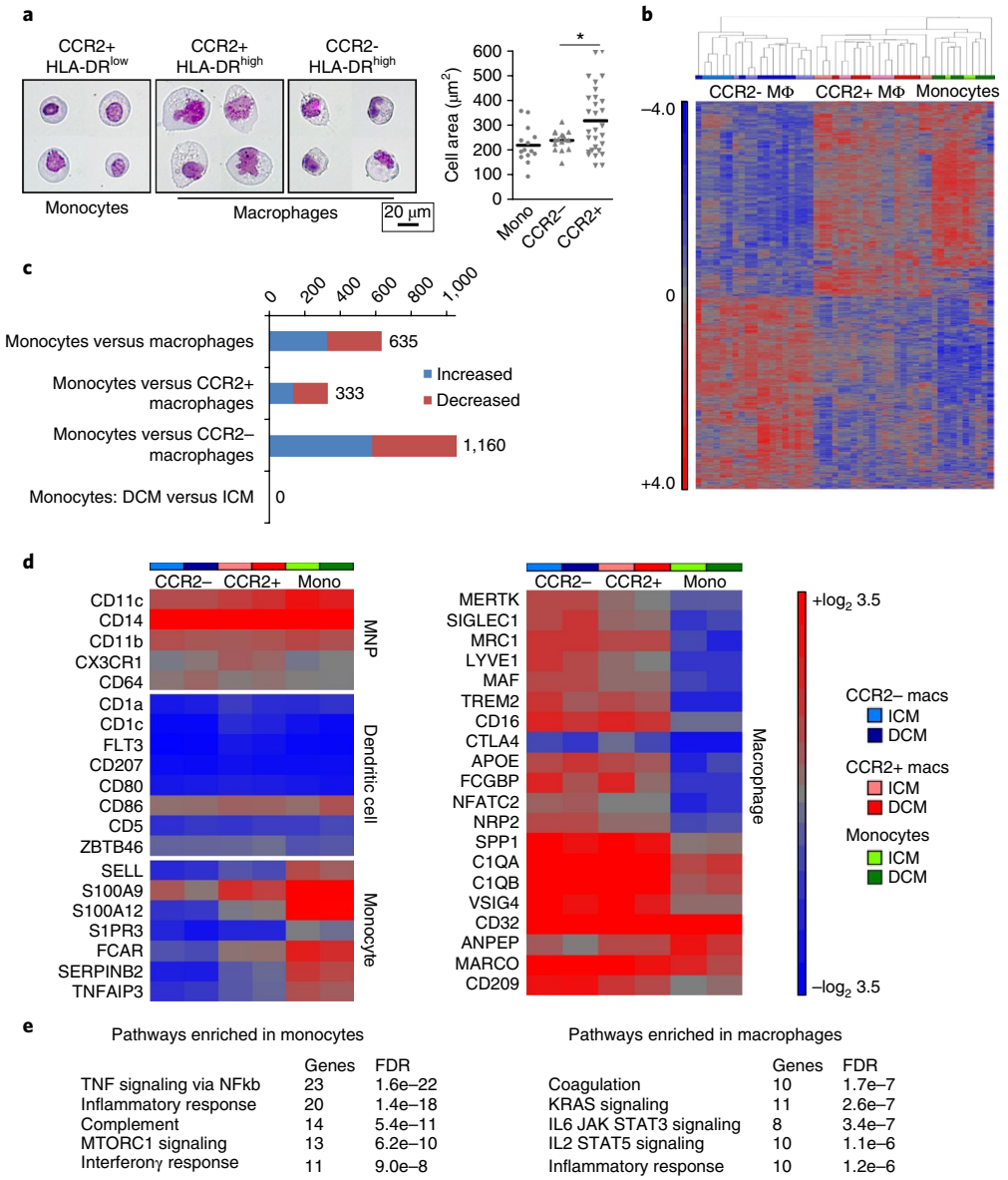

e

Pathways enriched in monocytes

	Genes	FDR
TNF signaling via NFkb	23	1.6e–22
Inflammatory response	20	1.4e–18
Complement	14	5.4e–11
MTORC1 signaling	13	6.2e–10
Interferonγ response	11	9.0e–8

Pathways enriched in macrophages

	Genes	FDR
Coagulation	10	1.7e–7
KRAS signaling	11	2.6e–7
IL6 JAK STAT3 signaling	8	3.4e–7
IL2 STAT5 signaling	10	1.1e–6
Inflammatory response	10	1.2e–6

Fig. 3 | Microarray gene expression profiling of CCR2+ monocytes, CCR2− macrophages, and CCR2+ macrophages in the failing human heart. a, Left, representative images of CCR2+HLA-DR^{low} monocytes ($n=14$), CCR2+HLA-DR^{high} macrophages ($n=16$), and CCR2−HLA-DR^{high} macrophages ($n=29$) isolated from four biologically independent failing hearts (ICM and DCM) using FACS. Wright staining; original magnification, ×800. Right, quantification of cell area. Asterisks denote $P<0.05$. Each data point represents an individual cell and the line represents the median value. Mann–Whitney test (two-sided) $P=0.025$. **b**, Hierarchical clustering highlighting the relationships among CCR2+ monocytes ($n=10$), CCR2− macrophages ($n=19$), and CCR2+ macrophages ($n=19$) in the failing heart (DCM, $n=8$ and ICM, $n=11$). Sample color scheme is identical to the legend in **d**. MΦ, macrophages. **c**, Bar graph displaying the number of differentially regulated genes, using a threshold of 2× fold change and FDR < 0.05. Comparisons include both DCM and ICM samples except when otherwise indicated. Blue, increased expression; red, decreased expression. **d**, Heat maps showing the absolute expression values of genes that are associated with human mononuclear phagocytes (MNPs), dendritic cells, monocytes, and macrophages. Data are shown for CCR2+ monocytes, CCR2− macrophages, and CCR2+ macrophages obtained from specimens of subjects with ICM or DCM and the results are displayed as average expression values. Mono, monocytes. **e**, GSEA pathway analysis revealing pathways enriched in cardiac monocytes versus macrophages. Analysis combines ICM and DCM specimens. Statistical significance was evaluated using FDR.

with our finding that monocytes exclusively contribute to maintenance of CCR2+ macrophages. Differential gene expression analysis revealed 635 genes that were differentially expressed between cardiac monocytes and macrophages (CCR2− and CCR2+) using a threshold of twofold change and false discovery rate (FDR) < 0.05. Consistent with our hierarchical cluster analysis, CCR2− macrophages had a greater number of genes ($n=1160$) that were differentially expressed compared to monocytes than did CCR2+ macrophages ($n=333$). Of note, no differentially expressed genes were identified in monocytes isolated from subjects with DCM versus ICM (Fig. 3c).

To place human cardiac monocytes and macrophages within the broader context of what is known regarding human myeloid populations, we examined the expression of previously described mononuclear phagocyte, dendritic cell, monocyte, and macrophage cell markers[20,24]. Consistent with previous reports describing

human mononuclear phagocytes, human cardiac CCR2+ monocytes, CCR2+ macrophages, and CCR2− macrophages uniformly expressed CD11c/ITGAX, CD14, CD11b/ITGAM, CX3CR1, and CD64/FCGR1. In contrast, human cardiac CCR2+ monocytes, CCR2+ macrophages, and CCR2− macrophages lacked the expression of numerous dendritic cell markers including CD1a, CD1c, FLT3, CD207/Langerin, CD80/B7, CD5, and ZBTB46. CCR2+ monocytes, CCR2+ macrophages, and CCR2− macrophages did express CD86, which is found on both macrophages and dendritic cells[25]. The previously reported monocyte cell markers SELL/L-selectin, S100A9, and S100A8 were differentially expressed on CCR2+ monocytes compared to CCR2− and CCR2+ macrophage subsets. Other identified genes differentially expressed by CCR2+ monocytes included S1PR3, FCAR, SERPINB2, and TNFAIP3. Consistent with macrophage cell identity, human cardiac CCR2− and CCR2+ macrophages displayed robust expression of MERTK, SIGLEC1, MRC1, LYVE1, MAF, TREM2, CD16, CD32, SPP1/Osteopontin, and MARCO (Fig. 3d). GSEA pathway analysis demonstrated that genes upregulated in monocytes displayed enrichment for pathways involved in TNF/NFκb signaling, inflammatory response, complement, MTORC1, and interferonγ signaling. In contrast, genes upregulated in macrophages displayed enrichment for pathways involved in coagulation, K-RAS, IL6/STAT3, IL2/STAT5, and inflammatory signaling (Fig. 3e).

To evaluate whether human cardiac CCR2− and CCR2+ macrophages represent functionally distinct subsets, we further examined our microarray data. Both hierarchical clustering (Fig. 3b) and principal component analysis (Fig. 4a) demonstrated that CCR2− and CCR2+ macrophages display distinct gene expression profiles. Differential gene expression analysis revealed 1,194 genes that were differentially expressed between CCR2− and CCR2+ macrophages using a threshold of 1.5-fold change and FDR < 0.05. Stratification by cardiomyopathy etiology (DCM versus ICM) revealed only six genes differentially regulated in CCR2+ macrophages and four genes differentially regulated in CCR2− macrophages, all of which were upregulated in ICM specimens (Fig. 4b). Genes upregulated in CCR2− macrophages included OR2A9P (pseudogene), SUV39H2 (Histone-lysine N-methyltransferase), G6PC3 (glucose-6-phosphatase catalytic subunit 3) and ST7-OT4 (non-coding RNA). Genes upregulated in CCR2+ macrophages included TEX37 (Testis Expressed 37), GNPDA (Glucosamine-6-Phosphate Deaminase 1), PLEKHA7 (Pleckstrin homology domain-containing family A member 7), L3MBTL4-AS1 (antisense RNA), THC2493232 (not characterized), and LNC-TWSG1-1 (non-coding RNA).

GSEA pathway analysis highlighted that genes upregulated in CCR2+ macrophages were associated with inflammatory pathways including TNF/NFκb signaling, inflammatory response, allograft rejection, IL2/STAT5, IL6/STAT3, interferonγ, hypoxia, and K-RAS signaling. In contrast, genes upregulated in CCR2− macrophages were associated with epithelial mesenchymal transition, coagulation, myogenesis, p53, and IL2/STAT5 signaling (Fig. 4c). To more precisely gauge the inflammatory potential of CCR2− and CCR2+ macrophage subsets, we examined known chemokines, immunomodulators, cytokines, and associated signaling pathways. Compared to CCR2− macrophages, which differentially expressed negative immunomodulators and tissue macrophage markers such as LILRB5, CD163, MRC1, MAF, SIGLEC1, and LYVE1, CCR2+ macrophages expressed large numbers of chemokines, chemokine receptors, and mediators of IL1, NFκb, and IL6 signaling. In contrast, CCR2− macrophages expressed numerous growth factors, extracellular matrix components, and conduction genes such as IGF1, PDGFC, EGFL7, GDF15, NRP1, SLIT3, ECM1, SDC3, SCN9A, and FGF13. CCR2+ macrophages expressed growth factors known to promote fibrosis and hypertrophy, including AREG, EREG, OSM, and PTX3[26–28], as well as genes associated with extracellular matrix degradation such as MMP9 and TIMP1 (Fig. 4d). Only some classic markers of M1 and M2 macrophage phenotypes were differentially expressed between CCR2− and CCR2+ macrophages, highlighting the limitations of this approach (Supplementary Fig. 4). Collectively, these data support the conclusion that CCR2+ monocytes, CCR2+ macrophages, and CCR2− macrophages represent distinct cell types and suggest that CCR2+ monocytes and CCR2+ macrophages likely represent inflammatory populations, while CCR2− macrophages are enriched with genes with the potential to orchestrate tissue repair.

CCR2+ macrophages represent an inflammatory population. To test the hypothesis that CCR2+ macrophages represent an inflammatory population, we purified CCR2− and CCR2+ macrophages from human left ventricular specimens using flow cytometry-based cell sorting and cultured cells in vitro. Macrophages were then treated with either vehicle control or the TLR4 agonist lipopolysaccharide (LPS). Using quantitative PCR with reverse transcription (RT-qPCR), we then measured messenger RNA expression of the pro-inflammatory mediators IL1β and CCL7. Following stimulation with either vehicle or LPS, CCR2+ macrophages expressed substantially higher levels of IL1β and CCL7 mRNA compared to CCR2− macrophages. While CCR2− macrophages did display increased IL1β and CCL7 mRNA expression following LPS treatment (compared to vehicle), the overall magnitude of IL1β and CCL7 mRNA expression was substantially lower than that of CCR2+ macrophages (Fig. 5a,b). Measurement of IL1β protein concentration in the cell culture supernatant further demonstrated that CCR2+ macrophages produce more IL1β than CCR2− macrophages (Fig. 5c).

To provide further evidence that human cardiac CCR2+ macrophages are pro-inflammatory, we developed a human organotypic slice culture system based on previously described reports[29,30]. Briefly, human heart explants were obtained from patients undergoing cardiac transplantation and the left ventricular lateral wall trimmed into transmural rectangular specimens. Using a Krumdieck Tissue Slicer, 300 µm tissue slices were generated and cultured on semiporous tissue culture inserts. TUNEL staining performed 2 h (baseline), 24 h, and 48 h after slice culture revealed that 0.5 ± 0.6, 11.5 ± 3.1, and 10.25 ± 3.0 cardiomyocytes per 20× field underwent cell death after 2 h, 24 h, and 48 h of slice culture, respectively (Fig. 5d,e). These data indicate that while the majority of cardiomyocytes remain viable after 48 h slice culture, foci of cardiomyocyte cell death reproducibly emerge within 24 h of slice culture. As such, we took advantage of this system to model how cardiac macrophage populations might respond to cardiomyocyte cell death ex vivo. While it is possible that macrophages may respond to other stimuli, this system allowed us to interrogate macrophage behavior in their native environment.

Consistent with previous studies in mouse models demonstrating that cardiomyocyte cell death results in cardiac macrophage activation and expression of pro-inflammatory mediators, immunostaining of human cardiac tissue slices cultured for 24 h revealed marked induction of IL1β expression in CD68+ macrophages compared to baseline (Fig. 5f, Supplementary Fig. 5). RT-qPCR further demonstrated robust increases in IL1β, CCL7, TNF, and IL10 mRNA expression in human cardiac tissue slices cultured for 24 h (Fig. 5g). Consistent with the conclusion that CCR2+ macrophages represent an inflammatory subset, IL1β expression specifically colocalized with CCR2+ CD68+ cells (Fig. 5h,i).

CCR2+ macrophage abundance is associated with persistent left ventricular systolic dysfunction following mechanical unloading. Given that human cardiac CCR2− and CCR2+ macrophages represent distinct macrophage subsets and likely have divergent functions, we hypothesized that these populations may differentially impact on cardiac function and left ventricular remodeling. To test this hypothesis, we examined whether human cardiac macrophage

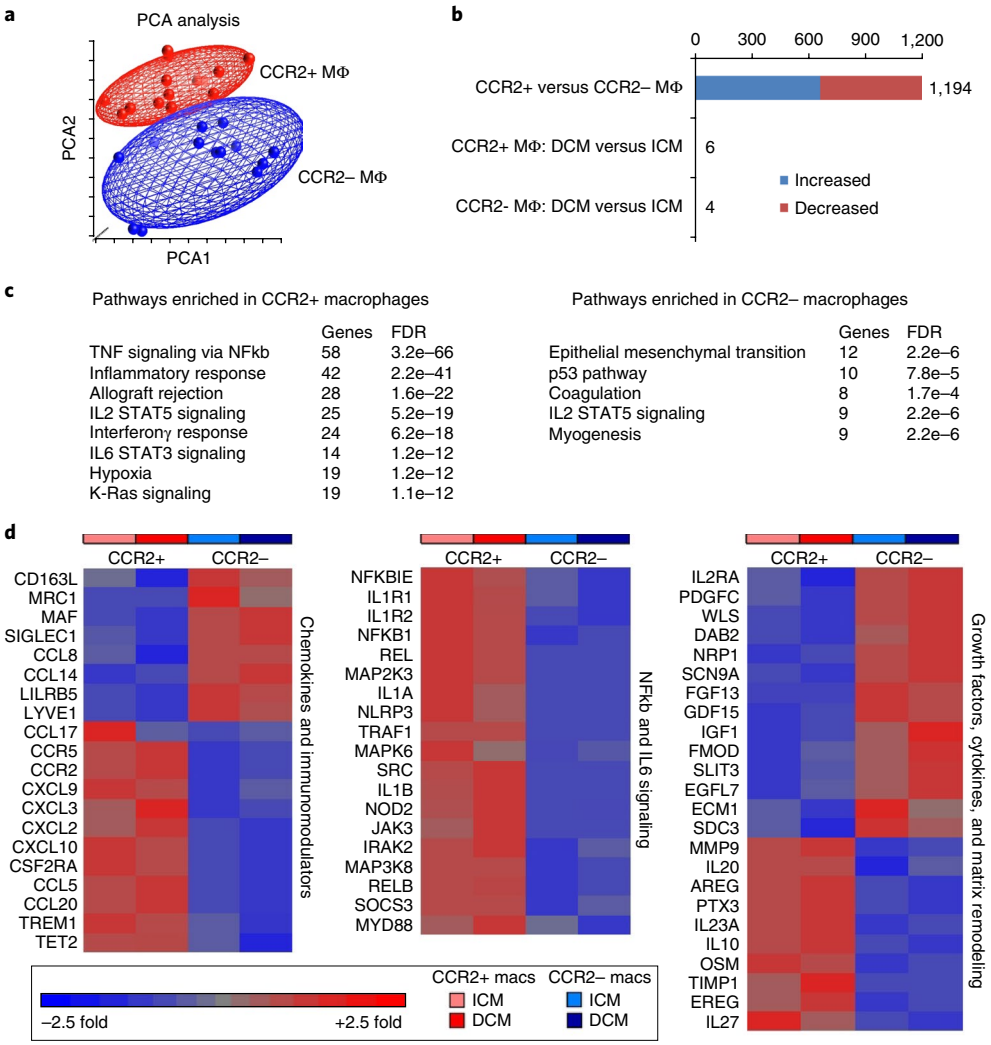

Fig. 4 | CCR2– and CCR2+ macrophages display distinct gene expression profiles. a, Principal component analysis of CCR2– ($n=19$) and CCR2+ ($n=19$) cardiac macrophages (ICM and DCM). Red, CCR2+ macrophages; blue, CCR2– macrophages. **b**, Bar graph displaying the number of genes that were differentially expressed between all CCR2– and CCR2+ macrophages (DCM and ICM) and the number of genes that were differentially expressed in CCR2– and CCR2+ macrophages, stratified by DCM and ICM designation using a threshold of 1.4 × fold change and FDR < 0.05. Blue, increased expression; red, decreased expression. **c**, GSEA pathway analysis revealing pathways enriched in cardiac CCR2+ versus CCR2– macrophages (ICM and DCM). Statistical significance was evaluated using FDR. **d**, Heat maps showing relative fold changes in genes associated with chemokine and immunomodulatory signaling, NFκb and IL6 signaling, as well as selected growth factors, cytokines, and extracellular matrix remodeling factors. Data are shown for CCR2+ and CCR2– macrophages obtained from specimens of subjects with ICM or DCM and the results are displayed as average expression values. All genes displayed on the heat maps were differentially expressed (FDR < 0.05) between CCR2+ and CCR2– macrophages.

subset composition was associated with left ventricular systolic function in a well described cohort of patients who underwent LVAD implantation[31,32]. Based on echocardiographic analysis, 34% of patients within this cohort displayed sustained improvements in left ventricular ejection fraction (> 50% relative increase) and reduced left ventricular volumes 6 months following LVAD implantation. Using immunostaining, we measured macrophage composition in left ventricular specimens obtained at the time of LVAD implantation ($n=36$) and at the time of transplantation ($n=26$). Subjects were stratified into two groups based on changes in left ventricular systolic function at 6 months as originally described: (1) persistent left ventricular dysfunction (< 50% relative improvement in left ventricular ejection fraction, $n=18$) and (2) improved left ventricular systolic function (> 50% relative increase in left ventricular ejection fraction or absolute ejection fraction > 40%, $n=18$) (Fig. 6a, Supplementary Fig. 6). Analysis of clinical and demographic data revealed balanced covariates between these groups and further showed that subjects who experienced improved left ventricular systolic function displayed concomitant reductions in left ventricular chamber dimensions (Supplementary Table 2).

Quantification of macrophage composition demonstrated that CD68+ macrophage abundance was not associated with improvements in left ventricular systolic function either at the time of LVAD implantation or transplantation (Fig. 6b). In contrast, both the abundance and percentage of CCR2+ macrophages correlated with left ventricular systolic function following LVAD implantation. Specifically, subjects who displayed improvement in left ventricular systolic function 6 months after LVAD implantation had lower absolute numbers and percentage of CCR2+ macrophages both at the time of LVAD implantation and at the time of explant (Fig. 6c,d). The percent of CCR2+ macrophages at the time of explant was associated with absolute changes in ejection fraction and left ventricular systolic dimension (Fig. 6e,f). Collectively, these findings suggest that cardiac macrophage composition is associated with left ventricular

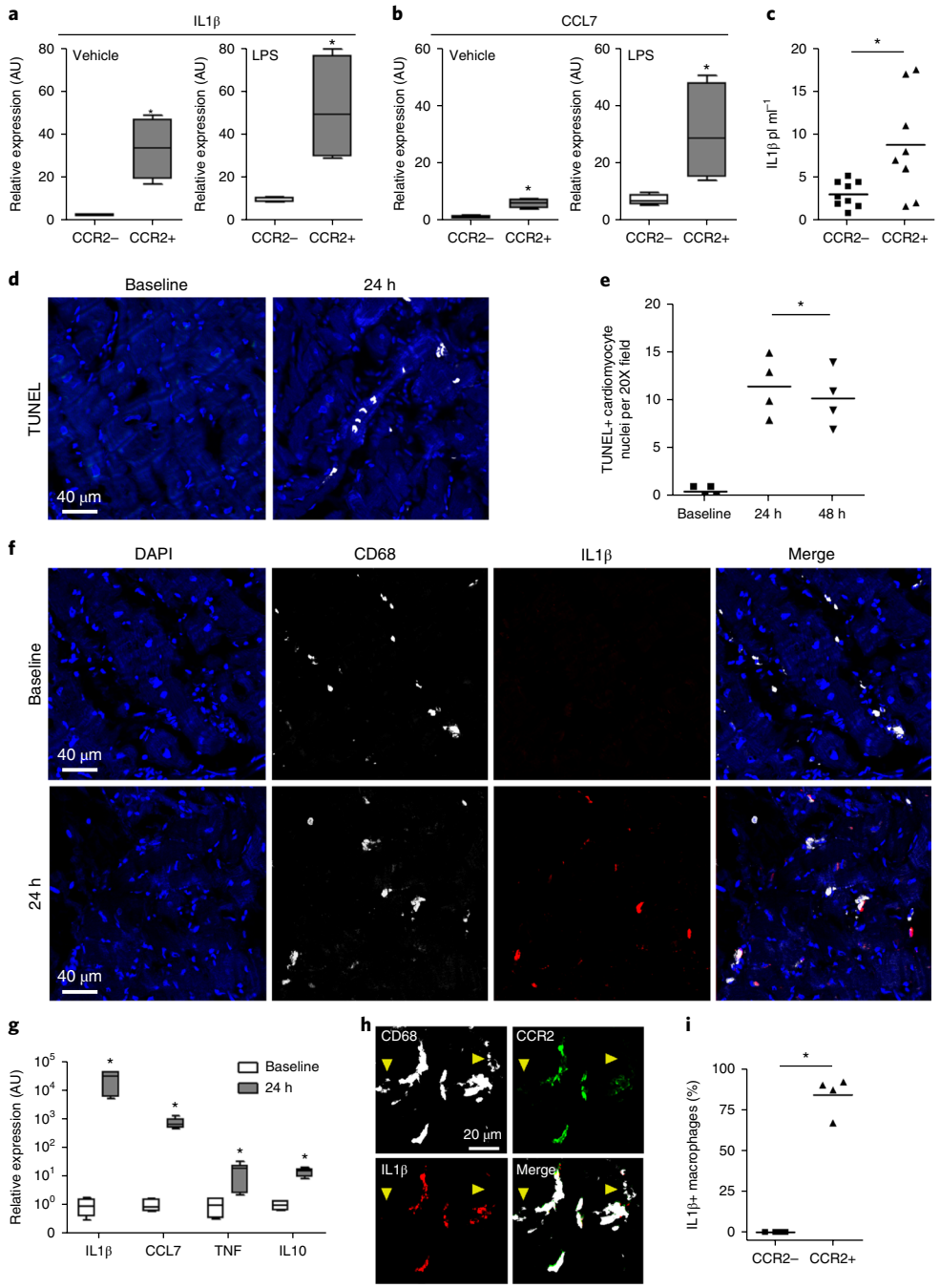

Fig. 5 | CCR2+ cardiac macrophages represent an inflammatory population. a,**b**, IL1β (**a**) and CCL7/MCP3 (**b**) expression in CCR2− and CCR2+ macrophages treated with vehicle or LPS, as assessed by RT-qPCR. Asterisks denote $P < 0.05$ (Mann–Whitney test, two-sided) compared to CCR2− macrophages. $n = 3$ independent experiments from four biologically independent heart failure specimens (DCM and ICM). Data are displayed as box and whisker plots. The box denotes the 25th and 75th percentiles, the line indicates the median value, and the whiskers reflect the minimum and maximum values. AU, arbitrary units. **c**, IL1β secretion by cultured CCR2− and CCR2+ macrophages, as assessed by enzyme-linked immunosorbent assay. Each data point represents a biologically independent replicate derived from four individual heart failure specimens (DCM and ICM). Line indicates the mean values. Asterisks denote $P < 0.05$ (Mann–Whitney test, two-sided). **d**,**e**, Cardiomyocyte cell death in the human myocardial slice culture system. **d**, Representative images of TUNEL staining showing evidence of cardiomyocyte cell death after 24 h slice culture. **e**, Quantification of TUNEL staining at 24 and 48 h of slice culture. Baseline refers to examination of myocardial tissue immediately after slice preparation. Asterisks denote $P < 0.05$ (analysis of variance) compared to baseline. Each data point ($n = 4$) is derived from a biologically independent heart failure specimen (DCM and ICM) and lines denote mean values. **f**, Immunostaining for CD68 (white) and IL1β (red) showing induction of IL1β expression in macrophages after 24 h slice culture. **g**, IL1β, CCL7/MCP3, TNF, and IL10 mRNA expression after 24 h slice culture. Data are displayed as box and whisker plots. The box denotes the 25th and 75th percentiles, the line indicates the median value, and the whiskers reflect the minimum and maximum values. Asterisks denote $P < 0.05$ (Mann–Whitney test) compared to baseline. $n = 3$ independent experiments. **h**, Immunostaining for CD68 (white), CCR2 (green), and IL1b (red) indicates that IL1β is preferentially expressed in CCR2+ macrophages. Yellow arrowheads, CCR2− macrophages. **i**, Percentages of CCR2− and CCR2+ macrophages with detectable IL1β antibody staining. Each symbol refers to data derived from a biologically independent heart failure specimen and lines indicate mean values. Asterisks denote $P < 0.05$ (Mann–Whitney test). **d**,**f**, Original magnification, ×200. **h**, Original magnification, ×400. Blue, DAPI.

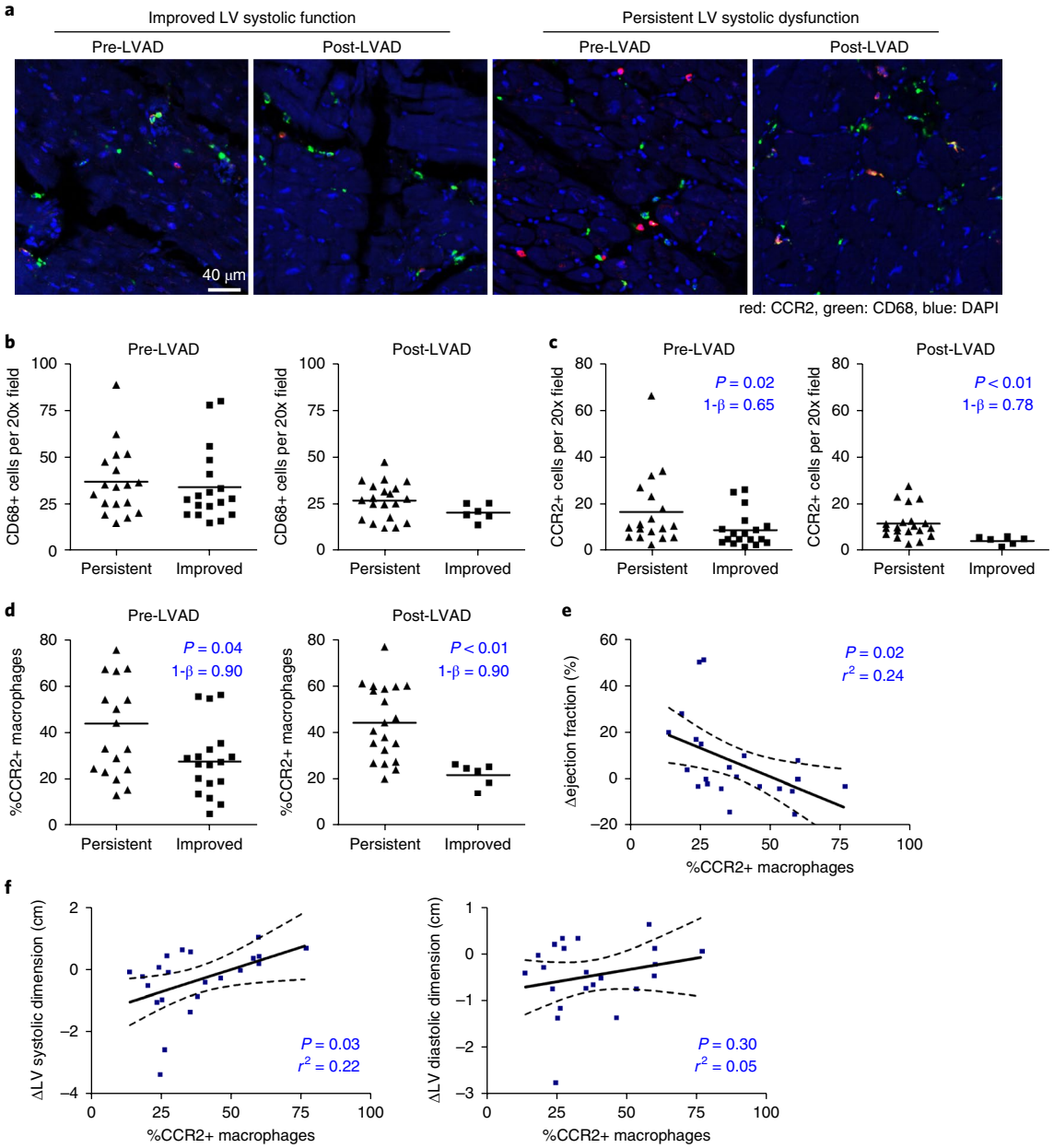

Fig. 6 | Macrophage subpopulations are associated with outcome following mechanical unloading. a, Immunostaining for CD68 (green) and CCR2 (red) in myocardial tissue specimens obtained from heart failure patients at the time of LVAD placement (pre-LVAD) and at the time of transplant (post-LVAD). Patients were stratified into those who displayed persistent left ventricular systolic dysfunction ($n=17$) and those who displayed improved left ventricular systolic function ($n=18$). Blue, DAPI; original magnification, ×200. LV, left ventricular. **b**,**c**, Numbers of total (CD68+) (**b**) and CCR2+ (**c**) macrophages in pre-LVAD and post-LVAD specimens. Mann–Whitney test (two-sided): CD68+ pre-LVAD, $P=0.40$ and CD68+ post-LVAD, $P=0.16$. **d**, Percentage of CCR2+ macrophages in pre-LVAD and post-LVAD. All data points represent biologically independent specimens and the lines indicate mean values. Asterisks indicate statistically significant P values using Mann–Whitney test (two-sided). **e**,**f**, Linear regression analysis for the association of the percentage of CCR2 macrophages and absolute changes in ejection fraction (**e**) and left ventricular systolic dimension (**f**) over time. Dashed lines indicate 95% confidence intervals. Asterisks denotes $P<0.05$. 1-β denotes statistical power. Each data point ($n=22$) represents a biologically independent sample.

systolic function and cardiac remodeling following mechanical unloading and support the concept that the human heart contains functionally distinct subsets of macrophages that may have clinically important effects on heart failure outcomes.

Discussion

The goal of this study was to determine whether emerging concepts of tissue macrophage heterogeneity are translatable to humans. By examining left ventricular myocardial specimens obtained from patients with heart failure, we tested the hypothesis that the human heart contains a heterogeneous population of macrophages with divergent origins and functions. We demonstrated that the human myocardium is populated by distinct subsets of CCR2− macrophages, CCR2+ macrophages, and CCR2+ monocytes. CCR2− macrophages represent a tissue-resident population that is maintained outside of monocyte input through local proliferation, while CCR2+ macrophages are likely derived from monocytes and expand locally through cell proliferation. Gene expression profiling, cell culture, and organotypic slice culture substantiated that CCR2− macrophages and CCR2+ macrophages represent distinct

cell types with divergent reparative and inflammatory functions, respectively. Consistent with a pathological role for CCR2+ macrophages, the abundance of CCR2+ macrophages was associated with persistent left ventricular systolic dysfunction and adverse left ventricular remodeling following mechanical unloading in heart failure patients. Collectively, these data demonstrate that the human heart contains distinct macrophage subsets that are functionally analogous to mouse CCR2− and CCR2+ macrophages and provide initial evidence that human macrophage heterogeneity is functionally important.

Paradigm-shifting studies have revealed that mice contain a complex and heterogeneous array of tissue macrophages with distinct origins, life cycles, and functions. We have previously demonstrated that mouse cardiac macrophage populations can be divided into CCR2−MHCII^{low}, CCR2−MHCII^{high}, and CCR2+MHCII^{high} subsets. Single cell RNA sequencing of mouse cardiac macrophages confirmed the presence of these subsets and suggested that CCR2 and MHCII expression is sufficient to resolve macrophage subset heterogeneity under homeostatic conditions[21]. CCR2− (MHCII^{low} and MHCII^{high}) macrophages are derived from embryonic progenitors (yolk sac and fetal monocytes), seed the heart during development, are maintained independent of monocyte input through local proliferation, possess minimal inflammatory potential, and display robust pro-angiogenic activity. In contrast, CCR2+ macrophages are derived from adult hematopoietic progenitors, maintained through CCR2+MHCII^{low}Ly6C^{high} monocyte recruitment and subsequent proliferation, and dramatically increase in number following cardiac tissue injury or in models of heart failure[8,17,22,33,34]. Recruited CCR2+MHCII^{low}Ly6C^{high} monocytes and CCR2+MHCII^{high} macrophages express a broad array of inflammatory mediators and contribute to heart failure progression through exaggerated neutrophil and monocyte recruitment, oxidative injury, and collateral tissue damage. Intriguingly, in the context of aging, monocyte-derived macrophages progressively replace embryonic-derived macrophages in some tissues including the heart[35].

Similar to mouse models, myocardial specimens obtained from subjects with DCM and ICM contained CCR2− macrophages, CCR2+ macrophages, and CCR2+ monocytes. These data are in line with previous reports that human monocytes and monocyte-derived macrophages express CCR2[36,37]. Consistent with mouse subsets, CCR2+ macrophages express high levels of the MHC class II homologue, HLA-DR, while CCR2+ monocytes express low levels of HLA-DR. One distinction between mouse and human macrophages is that mouse CCR2− macrophages are divided into MHCII^{low} and MHCII^{high} subsets, while human CCR2− macrophages are predominately HLA-DR^{high}. To date, beyond antigen presentation, no functional differences have been described between mouse CCR2−MHCII^{low} and CCR2−MHCII^{high} macrophages[8].

Human CCR2+ monocytes, CCR2+ macrophages, and CCR2− macrophages uniformly expressed common markers of monocytes and macrophages (CD14, CD64/FCGR1A, CD32/FCGR2A) and lacked the expression of known dendritic cell markers (ZBTB46, CD1a, CD1c, CD80, CD5, Flt3)[20,23,24]. CCR2+ monocytes within the heart express high levels of CD14 and low levels of CD16, suggesting that they may be most related to human blood CD14+ CD16− monocytes, the functional equivalent of mouse blood Ly6C^{high}CCR2+ monocytes[24]. The presence of CCR2+ monocytes within myocardial tissue is consistent with prior reports describing the ability of monocytes to retain their identity and survey antigens within tissue[10]. Consistent with the paradigm that macrophages can be distinguished from monocytes and dendritic cells based on the expression of MerK[20,23], human cardiac CCR2− macrophages and CCR2+ macrophages expressed MertK on the mRNA and protein level, while CCR2+ monocytes lacked MertK expression. Gene expression profiling identified additional markers that distinguished tissue macrophages from monocytes. CCR2− and CCR2+ macrophages differentially expressed SIGLEC1, MRC1, LYVE1, MAF, TREM2, CD16, APOE, FCGBP, NFATC2, and NRP2. CCR2+ monocytes differentially expressed SELL/CD62L, S100A12, FCAR, SERPINB2, and TNFAIP3. Whether these markers differentiate monocytes and tissue macrophages in other organs remains to be clarified.

To decipher the contribution of monocyte recruitment to the maintenance of human CCR2− and CCR2+ macrophages, we examined patients who underwent sex-mismatched heart transplantation (male subjects who received a female heart). Subjects had normal allograft function, were free from rejection, and underwent transplantation >1 year before routine surveillance endomyocardial biopsy. While transplant studies are influenced by exposure to immunosuppressive medications, this analysis revealed that, similar to mouse CCR2− macrophages, human CCR2− macrophages exist independent of monocyte input. In contrast, monocyte recruitment contributed to maintenance of at least a subset of human CCR2+ macrophages. Cell proliferation appeared to be an important mechanism for both CCR2− and CCR2+ macrophages. These data are consistent with described repopulation dynamics of mouse CCR2− and CCR2+ macrophage subsets. Of note, these findings do not provide meaningful information regarding the rate of CCR2+ macrophage turnover and thus do not exclude the possibilities that CCR2+ macrophages may represent a long-lived monocyte-derived population or that CCR2+ macrophages may represent a mixed population of newly recruited and long-lived monocyte-derived macrophages.

Gene expression profiling revealed several features that were shared between mouse and human cardiac macrophages. Both mouse and human CCR2− macrophage subsets expressed higher levels of tissue-resident macrophage markers (MRC1, CD163, SIGLEC1, LYVE1) and growth factors (IGF1, PDGF-C) compared to human and mouse CCR2+ macrophages. Human CCR2− macrophages differentially expressed several other growth factors and extracellular matrix genes implicated in tissue morphogenesis and remodeling. Consistent with a recently described role in electrical conduction[21], human CCR2− macrophages expressed the sodium channel SCN9A and sodium channel modulator FGF13. Conversely, human and mouse CCR2+ macrophages selectively expressed inflammatory mediators including monocyte and neutrophil chemokines, the inflammatory cytokine IL1β, and associated components of the inflammasome[8,17,19,21]. Human CCR2+ macrophages also differentially expressed several genes implicated in adverse cardiac remodeling including MMP9, TIMP1, PTX3, EREG, and OSM[26–28,38].

Consistent with a role for CCR2+ macrophages in inflammation, adverse remodeling, and heart failure pathogenesis, isolated CCR2+ macrophages produced robust quantities of IL1β following either LPS stimulation or exposure to necrotic cardiomyocytes. In contrast, mouse and human CCR2− macrophages displayed markedly less inflammatory activity[17]. Importantly, human CCR2+ macrophage abundance was associated with worsened left ventricular systolic dysfunction and adverse remodeling in heart failure subjects. Together, these observations suggest that interventions that target CCR2+ macrophages may represent a favorable approach to suppress inflammation and adverse remodeling in the context of heart failure. In addition, the finding that mouse and human CCR2+ macrophages are functionally analogous implies that dissecting mechanisms by which mouse CCR2+ macrophages are activated and exert their inflammatory effects is translationally relevant and will likely lead to critical insights into the development of effective strategies to intervene in the inflammatory functions of human CCR2+ macrophages.

Prior studies have provided clues to suggest that macrophage heterogeneity may be applicable to other human tissues. Examination of transplant recipients has suggested that admixtures

of resident and recruited macrophage populations exist in human skin and lung[39–42]. Further evidence supporting the existence of tissue-resident populations in the skin is provided by examination of patients with deficiencies in bone marrow myelopoiesis. Subjects carrying either GATA2 or biallelic IRF8 mutations demonstrate preservation of epidermal Langerhans cells and dermal macrophages despite marked impairments in peripheral monocyte and dendritic cell differentiation[43–45]. Outside of these early studies, little is known regarding human tissue mononuclear phagocyte diversity and function. Intriguingly, a recent study exploring human lung mononuclear phagocytes obtained from explanted lung specimens identified immense diversity among lung monocyte, macrophage, and dendritic cell subsets[46]. Future studies will undoubtedly delineate whether other human tissues harbor heterogeneous mononuclear phagocyte populations with unique or differing recruitment dynamics and functions.

We acknowledge that there are important limitations to our study. In contrast to mouse models, it is not possible to perform lineage tracing or detailed cell tracking studies in humans. As a result, we are not able to make any meaningful conclusions regarding macrophage ontogeny as it relates to embryonic or adult hematopoietic origins. However, by examining sex-mismatched transplant recipients, we are able to gain valuable insights into resident versus recruited populations. Even though in situ hybridization may underestimate the number of recipient-derived macrophages, we believe that the robust differences observed between populations indicate that CCR2− macrophages are a tissue-resident population and CCR2+ macrophages are replenished through monocyte recruitment. We also recognize that inferences regarding macrophage function are limited to gene expression, in vitro assays, and clinical associations in a relatively small-sized cohort of patients.

In conclusion, we have demonstrated that the human heart contains distinct macrophage subsets with differing repopulation dynamics and gene expression profiles that are functionally analogous to tissue-resident CCR2− and inflammatory monocyte-derived CCR2+ macrophages found in the mouse heart. Our findings provide evidence that macrophage heterogeneity is functionally important in the human heart and suggest that therapeutics targeting inflammatory functions of CCR2+ macrophages may represent a novel therapeutic target for patients with heart failure.

Methods

Methods, including statements of data availability and any associated accession codes and references, are available at https://doi.org/10.1038/s41591-018-0059-x.

Received: 26 October 2017; Accepted: 13 April 2018;
Published online: 11 June 2018

References

1. Van Furth, R. & Cohn, Z. A. The origin and kinetics of mononuclear phagocytes. *J. Exp. Med.* **128**, 415–435 (1968).
2. Volkman, A., Chang, N. C., Strausbauch, P. H. & Morahan, P. S. Differential effects of chronic monocyte depletion on macrophage populations. *Lab. Invest.* **49**, 291–298 (1983).
3. Sawyer, R. T., Strausbauch, P. H. & Volkman, A. Resident macrophage proliferation in mice depleted of blood monocytes by strontium-89. *Lab. Invest.* **46**, 165–170 (1982).
4. Ginhoux, F. et al. Fate mapping analysis reveals that adult microglia derive from primitive macrophages. *Science* **330**, 841–845 (2010).
5. Schulz, C. et al. A lineage of myeloid cells independent of Myb and hematopoietic stem cells. *Science* **336**, 86–90 (2012).
6. Yona, S. et al. Fate mapping reveals origins and dynamics of monocytes and tissue macrophages under homeostasis. *Immunity* **38**, 79–91 (2013).
7. Hashimoto, D. et al. Tissue-resident macrophages self-maintain locally throughout adult life with minimal contribution from circulating monocytes. *Immunity* **38**, 792–804 (2013).
8. Epelman, S. et al. Embryonic and adult-derived resident cardiac macrophages are maintained through distinct mechanisms at steady state and during inflammation. *Immunity* **40**, 91–104 (2014).
9. Guilliams, M. et al. Alveolar macrophages develop from fetal monocytes that differentiate into long-lived cells in the first week of life via GM-CSF. *J. Exp. Med.* **210**, 1977–1992 (2013).
10. Jakubzick, C. et al. Minimal differentiation of classical monocytes as they survey steady-state tissues and transport antigen to lymph nodes. *Immunity* **39**, 599–610 (2013).
11. Gordon, S. & Pluddemann, A. Tissue macrophages: heterogeneity and functions. *BMC Biol.* **15**, 53 (2017).
12. Boyer, S. W., Schroeder, A. V., Smith-Berdan, S. & Forsberg, E. C. All hematopoietic cells develop from hematopoietic stem cells through Flk2/Flt3-positive progenitor cells. *Cell Stem Cell* **9**, 64–73 (2011).
13. Hoeffel, G. et al. Adult Langerhans cells derive predominantly from embryonic fetal liver monocytes with a minor contribution of yolk sac–derived macrophages. *J. Exp. Med.* **209**, 1167–1181 (2012).
14. Sieweke, M. H. & Allen, J. E. Beyond stem cells: self-renewal of differentiated macrophages. *Science* **342**, 1242974 (2013).
15. Davies, L. C., Jenkins, S. J., Allen, J. E. & Taylor, P. R. Tissue-resident macrophages. *Nat. Immunol.* **14**, 986–995 (2013).
16. Wynn, T. A., Chawla, A. & Pollard, J. W. Macrophage biology in development, homeostasis and disease. *Nature* **496**, 445–455 (2013).
17. Lavine, K. J. et al. Distinct macrophage lineages contribute to disparate patterns of cardiac recovery and remodeling in the neonatal and adult heart. *Proc. Natl Acad. Sci. USA* **111**, 16029–16034 (2014).
18. Leid, J. et al. Primitive embryonic macrophages are required for coronary development and maturation. *Circ. Res.* **118**, 1498–1511 (2016).
19. Li, W. et al. Heart-resident CCR2 + macrophages promote neutrophil extravasation through TLR9/MyD88/CXCL5 signaling. *JCI Insight* **1**, e87315 (2016).
20. Xue, J. et al. Transcriptome-based network analysis reveals a spectrum model of human macrophage activation. *Immunity* **40**, 274–288 (2014).
21. Hulsmans, M. Macrophages facilitate electrical conduction in the heart. *Cell* **169**, 510–522 (2017).
22. Sager, H. B. et al. Proliferation and recruitment contribute to myocardial macrophage expansion in chronic heart failure. *Circ. Res.* **119**, 853–864 (2016).
23. Gautier, E. L. et al. Gene-expression profiles and transcriptional regulatory pathways that underlie the identity and diversity of mouse tissue macrophages. *Nat. Immunol.* **13**, 1118–1128 (2012).
24. Reynolds, G. Human and mouse mononuclear phagocyte networks: A tale of two species. *Front. Immunol.* **6**, 330 (2015).
25. Zarif, J. C. A phased strategy to differentiate human CD14 + monocytes into classically and alternatively activated macrophages and dendritic cells. *Biotechniques* **61**, 33–41 (2016).
26. Garlanda, C., Bottazzi, B., Bastone, A. & Mantovani, A. Pentraxins at the crossroads between innate immunity, inflammation, matrix deposition, and female fertility. *Annu. Rev. Immunol.* **23**, 337–366 (2005).
27. Fujiu, K. et al. A heart–brain–kidney network controls adaptation to cardiac stress through tissue macrophage activation. *Nat. Med.* **23**, 611–622 (2017).
28. Kubin, T. et al. Oncostatin M is a major mediator of cardiomyocyte dedifferentiation and remodeling. *Cell Stem Cell* **9**, 420–432 (2011).
29. Vickers, A. E. et al. Organ slice viability extended for pathway characterization: an in vitro model to investigate fibrosis. *Toxicol. Sci.* **82**, 534–544 (2004).
30. Brandenburger, M. et al. Organotypic slice culture from human adult ventricular myocardium. *Cardiovasc. Res.* **93**, 50–59 (2012).
31. Diakos, N. A. et al. Myocardial atrophy and chronic mechanical unloading of the failing human heart: implications for cardiac assist device-induced myocardial recovery. *J. Am. Coll. Cardiol.* **64**, 1602–1612 (2014).
32. Drakos, S. G. et al. Magnitude and time course of changes induced by continuous-flow left ventricular assist device unloading in chronic heart failure: insights into cardiac recovery. *J. Am. Coll. Cardiol.* **61**, 1985–1994 (2013).
33. Epelman, S., Lavine, K. J. & Randolph, G. J. Origin and functions of tissue macrophages. *Immunity.* **41**, 21–35 (2014).
34. Heidt, T. et al. Differential contribution of monocytes to heart macrophages in steady-state and after myocardial infarction. *Circ. Res.* **115**, 284–295 (2014).
35. Molawi, K. et al. Progressive replacement of embryo-derived cardiac macrophages with age. *J. Exp. Med.* **211**, 2151–2158 (2014).
36. Kaufmann, A., Salentin, R., Gemsa, D. & Sprenger, H. Increase of CCR1 and CCR5 expression and enhanced functional response to MIP-1 alpha during differentiation of human monocytes to macrophages. *J. Leukoc. Biol.* **69**, 248–252 (2001).
37. Weber, C. et al. Differential chemokine receptor expression and function in human monocyte subpopulations. *J. Leukoc. Biol.* **67**, 699–704 (2000).

38. Burchfield, J. S., Xie, M. & Hill, J. A. Pathological ventricular remodeling: mechanisms: part 1 of 2. *Circulation* **128**, 388–400 (2013).
39. Kanitakis, J., Petruzzo, P. & Dubernard, J. M. Turnover of epidermal Langerhans' cells. *N. Engl. J. Med.* **351**, 2661–2662 (2004).
40. Eguiluz-Gracia, I. et al. Long-term persistence of human donor alveolar macrophages in lung transplant recipients. *Thorax* **71**, 1006–1011 (2016).
41. Bittmann, I. et al. Cellular chimerism of the lung after transplantation. An interphase cytogenetic study. *Am. J. Clin. Pathol.* **115**, 525–533 (2001).
42. Haniffa, M. Differential rates of replacement of human dermal dendritic cells and macrophages during hematopoietic stem cell transplantation. *J. Exp. Med.* **206**, 371–385 (2009).
43. Dickinson, R. E. et al. Exome sequencing identifies GATA-2 mutation as the cause of dendritic cell, monocyte, B and NK lymphoid deficiency. *Blood* **118**, 2656–2658 (2011).
44. Hambleton, S. IRF8 mutations and human dendritic-cell immunodeficiency. *N. Engl. J. Med.* **365**, 127–138 (2011).
45. Bigley, V. et al. The human syndrome of dendritic cell, monocyte, B and NK lymphoid deficiency. *J. Exp. Med.* **208**, 227–234 (2011).
46. Desch, A. N. Flow cytometric analysis of mononuclear phagocytes in nondiseased human lung and lung-draining lymph nodes. *Am. J. Respir. Crit. Care Med.* **193**, 614–626 (2016).

Acknowledgements

We acknowledge the Translational Cardiovascular Biorepository at Washington University for providing cardiac tissue specimens. This project was made possible by funding provided from the Children's Discovery Institute of Washington University and St. Louis Children's Hospital (CH-II-2015-462, CH-II-2017-628), the Foundation for Barnes-Jewish Hospital (8038-88), and the NHLBI (R01 HL138466, R01 HL139714). K.J.L. is supported by National Institutes of Health (NIH) K08 HL123519 and Burroughs Welcome Fund (1014782). Histology was performed in the DDRCC advanced imaging and tissue analysis core supported by Grant #P30 DK52574. The Genome Technology Access Center in the Department of Genetics at Washington University School of Medicine is partially supported by NCI Cancer Center Support Grant #P30 CA91842 to the Siteman Cancer Center and by ICTS/CTSA Grant #UL1TR000448 from the National Center for Research Resources (NCRR), a component of the NIH, and NIH Roadmap for Medical Research. S.G.D. is supported by NHLBI R01 HL135121-01, AHA HF 16SFRN29020000-Project 1, and the Nora Eccles Treadwell Foundation. M.N. is supported by NIH HL139598 and the MGH Research Scholar Program. Y.L. is supported by NIH R01HL131908 and R01HL125655. D.K. is supported by NIH P01AI116501 and R01 HL094601, Veterans Administration Merit Review grant 1I01BX002730 and the Foundation for Barnes-Jewish Hospital. M.H. was supported by an MGH ECOR Tosteson and Fund for Medical Discovery Fellowship (2017A052660).

Author contributions

G.B. performed the flow cytometry, gene expression profiling, and macrophage in vitro assays. C.S. performed and analyzed the immunostaining experiments. A.I. provided cardiac specimens. N.W. assisted with quantitative data analyses. S.G.D., C.H.S., and T.S.S. provided cardiac specimens and clinical data for the LVAD patient cohort. G.B., D.K., M.H., M.N., S.E., Y.L., and A.B. assisted with study design, data interpretation, and manuscript production. K.J.L. was responsible for all aspects of this study including study design, experimental execution, data analysis, data interpretation, and manuscript production.

Competing interests

The authors declare no competing interests.

Additional information

Supplementary information is available for this paper at https://doi.org/10.1038/s41591-018-0059-x.

Reprints and permissions information is available at www.nature.com/reprints.

Correspondence and requests for materials should be addressed to K.J.L.

Publisher's note: Springer Nature remains neutral with regard to jurisdictional claims in published maps and institutional affiliations.

Methods

Study approval. This study was approved by the Washington University in St. Louis Institutional Review Board (#201305086). All subjects provided informed consent before sample collection and the experiments were performed in accordance with the approved study protocol.

Pathologic specimens used for immunostaining and flow cytometry. Cardiac tissue specimens were obtained from adult subjects with DCM (idiopathic and familial) and ICM undergoing LVAD implantation or cardiac transplantation. Subjects with secondary causes of DCM, including cardiac amyloidosis, cardiac sarcoidosis, viral myocarditis, giant cell myocarditis, peripartum cardiomyopathy, chemotherapy-associated cardiomyopathy, and complex congenital heart disease, were excluded from this study. In addition, subjects with established autoimmune disease, active infections, human immunodeficiency virus, and hepatitis C were excluded. Tissues consisted of transmural specimens obtained from the apical or lateral wall of the left ventricle. Explanted hearts were flushed by cannulating the left and right coronary artery ostia and perfusing 200 ml cold saline. LVAD apical cores were flushed by cannulating an epicardial vessel and perfusing 50 ml cold saline. Specimens were then immersed in cold saline and were either immediately flash frozen or fixed in 10% formalin upon collection to preserve tissue integrity.

Flow cytometry. To generate single cell suspensions, saline-perfused cardiac tissue specimens were finely minced and digested in DMEM with collagenase type 1 (450 U ml^{-1}), hyaluronidase (60 U ml^{-1}), and DNase I (60 U ml^{-1}) for 1 h at 37 °C. All enzymes were sourced from Sigma. Digested samples were then filtered through 40 µm cell strainers and washed with cold HBSS that was supplemented with 2% FBS and 0.2% BSA. Red blood cell lysis was performed with ACK lysis buffer (Thermo Fisher Scientific). Cells were washed with HBSS and resuspended in 100 µl FACS buffer (PBS containing 2% FBS and 2 mM EDTA). For monocyte and macrophage sorting, cells were then stained with CD45-PercpCy5.5 (2D1), CD14-PE (M5E2), CD64-FITC (10.1), CCR2-APC (K036C2), and HLA-DR APC/Cy7 (L243) at 4 °C for 30 minutes in the dark. Stained single cell suspensions were washed twice with FACS buffer and resuspended in a 0.35 ml volume. DAPI was used to exclude dead cells. For intracellular flow cytometry, myocardial tissue was processed as outlined above to generate a single cell suspension. Following labeling with appropriate cell surface antibodies, cells were fixed (PFA, Biolegend 420801) and permeabilized (Permeabilization Wash Buffer, Biolegend 421002) and stained for CD68. FACS analysis and sorting was performed on BD LSR II and BD FACSAria III platforms. A complete list of antibodies is shown in Supplementary Table 3.

Immunohistochemistry. Paraffin-embedded sections were dewaxed in xylene, rehydrated, endogenous peroxide activity quenched in 10% methanol and 3% hydrogen peroxide, processed for antigen retrieval by boiling in citrate buffer pH 6.0 containing 0.1% Tween-20, blocked in 1% BSA, and stained with the following primary antibodies overnight at 4 °C: CD68 (KP1, eBiosceince; 1:2,000), CCR2 (7A7, Abcam; 1:2,000), CD34 (Q/bend1, Abcam; 1:2,000), Collagen 1 (COL-1, Abcam; 1:2,000), IL-1β (NB600-633, NOVUS; 1:2,000), Ki67 (ab15580, Abcam; 1:1,000), CD14 (ab183322, Abcam; 1:2,000), CD64 (ab119843, Abcam; 1:4,000), iNOS (ab76198, Abcam; 1:1,000), and HLA-DR (clone L243, Biolegend; 1:1,000). The primary antibody was detected using biotin conjugated anti-mouse or anti-rabbit secondary antibodies (Vector Labs) in conjunction with streptavidin horseradish peroxidase (ABC Elite, Vector Labs). The PerkinElmer Opal Multicolor IHC system was utilized to visualize antibody staining per manufacturer protocol. TUNEL staining (Roche) was performed per manufacturer protocol. Immunofluorescence was visualized on a Zeiss confocal microscopy system. Macrophages were quantified by examining at least four similarly oriented sections from four independent samples in blinded fashion.

Microarray. To isolate RNA, macrophages were directly sorted into QLT buffer containing 2-mercaptoethanol and RNA isolated using the RNeasy Micro Kit (Qiagen) per manufacturer's instructions. Gene expression profiling was performed using microarray analysis in collaboration with the Genome Technology Access Core at Washington University. RNA was amplified using the WTA (Sigma) system and hybridized to Agilent 8×60 gene chips. Data analysis was performed using Partek genome suite software.

Transplant specimens and in situ hybridization. To identify sex-mismatched patients who underwent cardiac transplantation, we performed a retrospective analysis of all patients who either received a cardiac transplant at Barnes-Jewish Hospital between 1994 and 2008 or received a heart transplant elsewhere and were followed in our post-transplant program between 1994 and 2008. Male subjects who received a heart from a female donor were included. Exclusion criteria included any episode of > 2R/3A rejection, prior or ongoing antibody-mediated rejection, established cardiac allograft vasculopathy, or left ventricular ejection fraction < 60%. Standard demographic information was obtained from the medical record including age, sex, reason for transplantation, cardiovascular comorbidities, transplant and heart failure medicines, rejection episodes, cytomegalovirus status, blood type, echocardiographic data, stress testing, left ventricular end diastolic pressure, heart rate, and blood pressure as derived from diagnostic catheterization data.

Myocardial biopsy specimens that were previously collected for routine clinical care were obtained from the department of pathology. Collected tissues were previously fixed in 10% formalin and stored in paraffin blocks. For each subject, the most recent biopsy specimen was obtained. Myocardial biopsy specimens were cut into 4-µm sections using standard techniques and mounted on glass slides. Each paraffin block typically contained 3–4 myocardial specimens. Immunohistochemistry was performed for CCR2 and CD68 as outlined above using the PerkinElmer Opal Multicolor IHC Kit. In situ hybridization for Y chromosomes (STARFISH) was performed after immunohistochemistry using a biotinylated probe per manufacturer's instructions. The biotin conjugated probe was detected using streptavidin-FITC and visualized on a Zeiss confocal microscopy system. Macrophages were quantified by examining at least four sections from each independent sample in blinded fashion.

Organotypic slice culture. To prepare cardiac slices, Krumdieck Tissue Slicer (Alabama Research and Development) was used. Tissue was first placed in a tissue embedding unit containing 4% low melting agarose dissolved in HBSS and allowed to set at 4 °C. The embedding unit was then placed onto the sample holder of the microtome assembly. The reservoir was filled with ice cold HBSS (without calcium and magnesium). The arm and blade speed were set to medium speed, and thickness of the slices was set to 300 µm. Following slice generation and collection, slices were then cultured at a liquid–air interface using semiporous tissue culture inserts (Millipore). Inserts containing cardiac tissue slices were placed in a six-well tissue culture plate with 1 ml IMDM supplemented with 20% FBS and 1% penicillin/streptomycin. Slices were cultured for 24–48 h at 37 °C in humidified air with 5% CO_2.

Macrophage cell culture. CCR2+ and CCR2− macrophages were purified from myocardial tissue using flow cytometry as described above. Cells were sorted on a BD FACSAria III platform with 85 µm nozzle and flow rate set to 1 µl min^{-1}. The pre- and post-sort collection tube holders were maintained at 4 °C to preserve cell viability. Cells were sorted directly into culture medium (DMEM supplemented with 10% FBS and 1% penicillin/streptomycin) and immediately plated into 96-well tissue culture plates and allowed to adhere overnight. The following day, fresh medium was added and cells were stimulated with vehicle control or LPS (10 ng ml^{-1}) for 6 h. IL1β concentration in the tissue culture supernatant was measured using the human IL1β Quantikine HS ELISA Kit (R&D Systems).

cDNA amplification and RT-PCR. RNA was extracted from the cardiac slices or cultured cells using the RNeasy RNA micro kit (Qiagen). RNA concentration was measured using a nanodrop spectrophotometer (ThermoFisher Scientific). For cardiac slices, cDNA synthesis was performed using the High Capacity RNA to cDNA synthesis kit (Applied Biosystems). For cultured macrophages, cDNA was synthesized using the iScript Reverse Transcription Supermix (Bio-Rad) and pre-amplified using the Sso Advanced PreAmp Supermix kit (Bio-Rad). Quantitative real-time PCR reactions were prepared with sequence-specific primers (IDT) with PowerUP Syber Green Master mix (ThermoFisher Scientific) in a 20 µl volume. Real-time PCR was performed using QuantStudio 3 (ThermoFisher Scientific). mRNA expression was normalized to β2 microglobulin (B2M). IL-1β: forward ATG CAC CTG TAC GAT CAC TG, reverse ACA AAG GAC ATG GAG AAC ACC; CCL7: forward AGA CCA AAC CAG AAA CCT CC, reverse AGT ATT AAT CCC AAC TGG CTG AG; IL-10: forward CGC ATG TGA ACT CCC TGG, reverse TAG ATG CCT TTC TCT TGG AGC; TNF: forward ACT TTG GAG TGA TCG GCC, reverse GCT TGA GGG TTT GCT ACA AC; β2M: forward TGC TGT CTC CAT GTT TGA TGT ATC T, reverse TCT CTG CTC CCC ACC TCT AAG.

Statistical analysis. Fisher's exact and Mann–Whitney tests were used to identify statistically significant differences between groups. Data are presented as dot plots, box whisker plots, or linear regression plots generated in PRISM. The exact sample size used to calculate statistical significance is stated in the appropriate figure legend. Replicates were defined as individual human specimens or experiments and described in the figure legends.

Reporting Summary. Further information on experimental design is available in the Nature Research Reporting Summary linked to this article.

Data Availability. Source Data for all experiments have been provided. All other data are available from the corresponding author on reasonable request. Microarray data were deposited in GEO (GSE112630). Additional details can be found in the Life Sciences Reporting Summary.

nature research

Corresponding author(s): Kory Lavine

Reporting Summary

Nature Research wishes to improve the reproducibility of the work that we publish. This form provides structure for consistency and transparency in reporting. For further information on Nature Research policies, see Authors & Referees and the Editorial Policy Checklist.

Statistical parameters

When statistical analyses are reported, confirm that the following items are present in the relevant location (e.g. figure legend, table legend, main text, or Methods section).

n/a	Confirmed	
☐	☒	The exact sample size (*n*) for each experimental group/condition, given as a discrete number and unit of measurement
☐	☒	An indication of whether measurements were taken from distinct samples or whether the same sample was measured repeatedly
☐	☒	The statistical test(s) used AND whether they are one- or two-sided *Only common tests should be described solely by name; describe more complex techniques in the Methods section.*
☐	☒	A description of all covariates tested
☒	☐	A description of any assumptions or corrections, such as tests of normality and adjustment for multiple comparisons
☐	☒	A full description of the statistics including central tendency (e.g. means) or other basic estimates (e.g. regression coefficient) AND variation (e.g. standard deviation) or associated estimates of uncertainty (e.g. confidence intervals)
☐	☒	For null hypothesis testing, the test statistic (e.g. *F*, *t*, *r*) with confidence intervals, effect sizes, degrees of freedom and *P* value noted *Give P values as exact values whenever suitable.*
☒	☐	For Bayesian analysis, information on the choice of priors and Markov chain Monte Carlo settings
☒	☐	For hierarchical and complex designs, identification of the appropriate level for tests and full reporting of outcomes
☒	☐	Estimates of effect sizes (e.g. Cohen's *d*, Pearson's *r*), indicating how they were calculated
☐	☒	Clearly defined error bars *State explicitly what error bars represent (e.g. SD, SE, CI)*

Our web collection on statistics for biologists may be useful.

Software and code

Policy information about availability of computer code

Data collection	data collection was performed manually
Data analysis	GraphPad Prism 7 and SAS for all statistical analyses. FlowJo v7.6.5. for FACS and Partek Genome Suite was used for microarray analysis

For manuscripts utilizing custom algorithms or software that are central to the research but not yet described in published literature, software must be made available to editors/reviewers upon request. We strongly encourage code deposition in a community repository (e.g. GitHub). See the Nature Research guidelines for submitting code & software for further information.

Data

Policy information about availability of data

All manuscripts must include a data availability statement. This statement should provide the following information, where applicable:

- Accession codes, unique identifiers, or web links for publicly available datasets
- A list of figures that have associated raw data
- A description of any restrictions on data availability

Provide your data availability statement here.

Field-specific reporting

Please select the best fit for your research. If you are not sure, read the appropriate sections before making your selection.

☒ Life sciences ☐ Behavioural & social sciences

For a reference copy of the document with all sections, see nature.com/authors/policies/ReportingSummary-flat.pdf

Life sciences

Study design

All studies must disclose on these points even when the disclosure is negative.

Sample size	Sample sizes were chosen based on specimen availability. We targeted a sample size of n>10 to account for sample variability.
Data exclusions	We did not exclude any data.
Replication	All experiments were reproduced at least 3 times. All attempts at replication were successful.
Randomization	When comparing between groups, samples were randomly assigned.
Blinding	Investigators quantifying data were blinded to group allocation during the analysis and measurement procedures.

Materials & experimental systems

Policy information about availability of materials

n/a	Involved in the study
☒	☐ Unique materials
☐	☒ Antibodies
☒	☐ Eukaryotic cell lines
☒	☐ Research animals
☐	☒ Human research participants

Antibodies

Antibodies used	Flow cytometery antibodies are listed in Supplemental Figure 3. Immunostaining antibodies: CD68 (KP1 eBiosceince 1:2000), CCR2 (7A7 Abcam 1:2000), CD34 (Q/bend1 Abcam 1:2000), Collagen 1 (COL-1 Abcam 1:2000), IL-1β (NB600-633 NOVUS 1:2000), Ki67 (ab15580 Abcam 1:1000), CD14 (ab183322 Abcam 1:2000), CD64 (ab119843 Abcam 1:4000), iNOS (ab76198 Abcam 1:1000), HLA-DR (clone L243 Biolegend 1:1000).
Validation	All antibodies were commercially available and validated in our laboratory using isotype controls.

Human research participants

Policy information about studies involving human research participants

Population characteristics	Recruitment of human research participants, covariate data collection, and analysis is described in the methods section. Relevant covariates (age, sex, race, heart failure etiology, diabetes, hypertension, echocardiographic parameters) are displayed in Supplemental Tables 1 and 2.

Method-specific reporting

n/a	Involved in the study
☒	☐ ChIP-seq
☐	☒ Flow cytometry
☒	☐ Magnetic resonance imaging

Flow Cytometry

Plots

Confirm that:

☒ The axis labels state the marker and fluorochrome used (e.g. CD4-FITC).

☒ The axis scales are clearly visible. Include numbers along axes only for bottom left plot of group (a 'group' is an analysis of identical markers).

☒ All plots are contour plots with outliers or pseudocolor plots.

☒ A numerical value for number of cells or percentage (with statistics) is provided.

Methodology

Sample preparation	Sample preparation is described in detail in the methods section. To generate single cell suspensions, saline perfused cardiac tissue specimens were finely minced, and digested in DMEM with Collagenase type 1 (450 U/ml) Hyaluronidase (60 U/ml) and DNase I (60 U/ml) for 1 hour at 37°C. All enzymes were sourced from Sigma. Digested samples were then filtered through 40 µM cell strainers and washed with cold HBSS that was supplemented with 2% FBS and 0.2% BSA. Red blood cell lysis was performed with ACK lysis buffer (Thermo Fisher Scientific). Cells were washed with HBSS and resuspended in 100 µL of FACS buffer (DPBS containing 2% FBS and 2 mM EDTA).
Instrument	BD Lsr II and BD Aria III
Software	FlowJo
Cell population abundance	The relevant cell populations represent 40-50% of CD45+ immune cells within the heart.
Gating strategy	Gating strategy is displayed in Figure 1c

☒ Tick this box to confirm that a figure exemplifying the gating strategy is provided in the Supplementary Information.